Supporting Information

Kopf et al. 10.1073/pnas.1512057112

SI Introduction

Using Stable Isotope Tracers to Measure Microbial Activity. This section provides an introduction to the equations describing isotopic enrichment in microbial populations exposed to an isotope tracer. Here we focus all nomenclature on the hydrogen isotope system only, although most equations are more broadly applicable.

The production and removal of biomass from a microbial population (B) is governed by the specific growth rate μ (which signifies cellular replication), turnover rate ω (which describes biosynthesis in excess of growth to compensate for degradation and turnover of macromolecules), and death/degradation rate d. The set of differential equations describing the rate of change in total biomass (dB/dt) and the rate of change in new biomass (dB_{new}/dt) is the difference between the synthesis and removal fluxes,

$$\begin{aligned}\frac{dB}{dt} &= (\mu+\omega-\omega-d)\cdot B = (\mu-d)\cdot B\\ \frac{dB_{new}}{dt} &= (\mu+\omega)\cdot B-(d+\omega)\cdot B_{new}.\end{aligned} \quad [S1]$$

A differential equation for the fraction of new vs. total biomass $[f_{B_{new}} = (B_{new}/B)]$ is derived using the quotient rule

$$\begin{aligned}\frac{df_{B_{new}}}{dt} &= \frac{\partial}{\partial t}\left(\frac{B_{new}}{B}\right) = \frac{1}{B}\frac{dB_{new}}{dt}-\frac{B_{new}}{B^2}\frac{dB}{dt}\\ &= \frac{1}{B}\left(\frac{dB_{new}}{dt}-f_{B_{new}}\frac{dB}{dt}\right)\\ &= (\mu+\omega)-f_{B_{new}}(d+\omega)-f_{B_{new}}(\mu-d)\\ &= \left(1-f_{B_{new}}\right)\cdot(\mu+\omega).\end{aligned} \quad [S2]$$

Integration provides a solution for $f_{B_{new}}(t)$ and its derivative $f'_{B_{new}}(t)$,

$$\begin{aligned}f'_{B_{new}}(t) &= (\mu+\omega)\cdot e^{-(\mu+\omega)\cdot t}\\ f_{B_{new}}(t) &= 1-e^{-(\mu+\omega)\cdot t}.\end{aligned} \quad [S3]$$

Now, in the case of a population exposed to an isotope tracer (for example, water enriched in deuterium – ^2H) starting at some time t_0, all biomass that is newly produced after addition of the tracer will have a distinct hydrogen isotope composition ($^2F_{B_{new}}$) reflecting the tracer. Mass balance between the newly produced and original biomass determines the overall isotopic composition,

$$^2F_B(t) = \frac{B_{new}}{B}\cdot {}^2F_{B_{new}} + \frac{B_{original}}{B}\cdot {}^2F_{B_{original}}. \quad [S4]$$

In the most basic scenario where new biomass simply reflects the isotopic composition of the tracer (here the spiked water, $^2F_{B_{new}} = {}^2F_{w_{spiked}}$), and there is no maintenance turnover ($\omega = 0$), this yields the following link between isotopic enrichment and growth (27, 51):

$$^2F_B(t) = {}^2F_{w_{spiked}}\cdot\left(1-e^{-\mu\cdot t}\right) + {}^2F_{B_{original}}\cdot e^{-\mu\cdot t}. \quad [S5]$$

This relationship between the isotopic enrichment and growth is illustrated in Fig. 1*A*, which shows the evolution of total biomass, new biomass, and old biomass over the course of two generation times (the biomass is not necessarily doubling, so these are only the apparent generation times) for varying death/removal rates. As should be apparent from Eq. **S5** and Fig. 1*A*, one important advantage of tracking growth by isotope tracer is that the effective pool size (B) of the microbial biomass does not affect the enrichment. This holds true even for the more complex scenarios that are relevant to this study and are derived in detail in Data processing for the analysis of clinical samples.

Minimum Incubation Times for Microbial Activity Detection. The estimated minimum incubation time requirements illustrated in Fig. 1*B* are calculated from Eq. **S5** as described previously (27), and are based on isotope labeling with 20% (vol/vol) ^2H_2O. Briefly, substituting the generation time for the growth rate $[\mu = (ln2/T)]$ and solving Eq. **S5** for the time t_{label} required to reach a final hydrogen isotope enrichment of $^2F_B(t_{label}) = {}^2F_{B_{final}}$ after addition of isotopically heavy water yields

$$t_{label} = \frac{T}{ln\ 2}\cdot ln\left(\frac{{}^2F_{w_{spiked}} - {}^2F_{B_{original}}}{{}^2F_{w_{spiked}} - {}^2F_{B_{final}}}\right) \quad [S6]$$

with $^2F_{w_{spiked}} = 20\%$, and the isotopic composition of the original biomass before spiking approximated by natural abundance hydrogen isotope values ($^2F_{B_{original}} = {}^2F_{nat} = 0.015574$ atom%). It is important to note that although the hydrogen isotopic composition of new biomass reflects the hydrogen isotope composition of source water in most experimental systems, it typically has a proportionality factor lower than unity (i.e., $^2F_{B_{new}} = \alpha\cdot {}^2F_{w_{spiked}}$ with $\alpha < 1$). Such lower values of α would lead to longer incubation time requirements than those reported in Fig. 1*B*, which reflect the idealized minimal incubation time requirements.

SI Materials and Methods

Laboratory Growth Media. For all growth experiments in a simulated complex medium in the laboratory, *S. aureus* (MN8) (52) was grown in a defined SCFM. This medium is designed to mimic the average nutritional environment of the CF lung, and was chosen as a representative model medium that simulates a clinical context more closely. The medium was prepared as previously described (20); briefly, SCFM is a Mops buffered medium (adjusted to pH 6.8) that contains basic salts, a mixture of amino acids (about ∼19 mM equivalents in total), glucose (3.2 mM), and lactate (9.3 mM). Due to the high concentration of amino acids, microbial growth in this medium tends to raise the pH significantly (pH > 8), and the medium was buffered with 50 mM instead of 10 mM Mops in this study. SCFM was further amended with vitamins required by *S. aureus*: 100 μ g/L thiamine (B1), 100 μ g/L nicotinic acid (B3), and 10 μ g/L biotin (B7). All culturing experiments were conducted aerobically at 37 °C with agitation, and were inoculated from fresh cultures grown on the same medium. Growth was monitored by measuring optical density at 600 nm. Cells intended for lipid analysis were generally harvested by centrifugation at 5,000 × *g* for 10 min (at 4 °C), washed by resuspension in 1× PBS solution, repelleted, and frozen immediately at −80 °C until lipid extraction and analysis.

Biological Considerations for the Experimental Approach. As outlined in Fig. 2, several biological considerations are important for evaluating the applicability of our experimental approach: the importance of biomarker specificity (consideration a), de novo biomarker synthesis (consideration b), and isotope label tolerance (consideration c). Here, we present data collected to address these aspects.

Evaluating biomarker specificity. Quantifying the anabolic activity of a specific target organism in a complex environment is only possible if a suitable biomarker for the organism of interest can be identified. In the context of a polymicrobial infectious disease within the human host, this requires a biomarker that can be distinguished from molecules produced both by the host itself and by other dominant pathogens. The fatty acids targeted in this study (the anteiso methyl branched C_{14} and C_{16} saturated fatty acids, *a*-$C_{15:0}$ and *a*-$C_{17:0}$) are synthesized specifically by *S. aureus* and can be distinguished from the host and most other dominant CF pathogens (Fig. S1).

Testing for de novo biomarker synthesis. Recycling exogenous sources is an important limitation to isotope labeling experiments in substrate-rich environments. If organisms can build their membranes from preexisting fatty acids, or fatty acid fragments, that are available in their environment, they no longer need to synthesize all fatty acids de novo. Consequentially, an isotopic tracer in the form of ^{2}H-rich water would be incorporated into the total membrane at a much slower rate. Without knowledge of the ability to recycle and rate of recycling, isotopic enrichment could underestimate true growth of the population, because growth with recycled fatty acids does not incorporate the tracer.

Two examples for this process are provided by recent work on this topic in *P. aeruginosa* (53, 54). First, the organism appears capable of recycling exogenous free fatty acids, such as C16:0, by direct incorporation *en bloc* during phospholipid biosynthesis. Any fatty acid recycled by this mechanism would carry its original isotopic signature from when it was first synthesized rather than incorporate any water isotope label present at the time of *en bloc* incorporation. Second, *P. aeruginosa* appears capable of reelongating partially degraded exogenous fatty acids. Typically, the initiating step of fatty acid synthesis from acetyl-CoA is catalyzed by ß-acetoacetyl-ACP synthase (*fabH* in *Escherichia coli*). In *P. aeruginosa*, however, a closely related but distinct new class of synthases (now called *fabY*) catalyze this step (54). Additionally, a wide range of genetically very similar enzymes exist in *P. aeruginosa*, and, even with a deletion mutant of *fabY*, the organism is capable of growing. Ref. 53 discovered that in the absence of *fabY*, the preferred fatty acid synthesis pathway initiated from acetyl-CoA (which is no longer possible without the gene) can be replaced in the presence of exogenous fatty acids (C_8, C_{12}, C_{16}, and undefined mixtures like LB). *P. aeruginosa* can simply shunt C_8-CoA from β-oxidation degradation of fatty acid metabolism back into fatty acid biosynthesis via the enzyme encoded by ORF PA3286, thereby skipping the de novo synthesis of the C_8 precursor carbon skeleton. From the scavenged intermediate, the organism can produce all longer-chain cellular fatty acids, including both saturated and unsaturated fatty acids. Any fatty acid recycled by this mechanism would carry a mixed isotopic signature with the C_8 tail maintaining its original isotopic composition, whereas the de novo elongated remainder of the molecule would reflect the water isotope label present at the time of reelongation.

We investigated whether *S. aureus,* the target organism of this study, is capable of recycling exogenous fatty acids it might encounter in the lung environment. Two commercially available perdeuterated precursor fatty acids (the naturally abundant octadecanoic acid and the only microbially produced pentadecanoic acid, both entirely ^{2}H-substituted in the hydrocarbon tail) were provided as an exogenous source of free fatty acids to test for recycling by *S. aureus*. Experiments were carried out in batch culture in 250-mL flasks with 100 mL of a defined phosphate buffered minimal medium [pH 7.2, 2.5 g/L NaCl, 13.5 g/L K_2HPO_4, 4.7 g/L KH_2PO_4, 1 g/L K_2SO_4, 0.1 g/L $MgSO_4 \cdot 7H_2O$, 10 mM NH_4Cl, 10 mM glycerol, 100 μ g/L thiamine (B1), 100 μ g/L nicotinic acid (B3), 10 μ g/L biotin, 11.5 mg/L proline, and 10 mL/L 50× MEM Amino Acid solution (M5550; Sigma-Aldrich), with final amino acid concentrations 63.2 mg/L arginine, 15.6 mg/L cysteine, 21 mg/L histidine, 26.35 mg/L isoleucine, 26.2 mg/L leucine, 36.3 mg/L lysine, 7.6 mg/L methionine, 16.5 mg/L phenylalanine, 23.8 mg/L threonine, 5.1 mg/L tryptophan, 18.0 mg/L tyrosine, 23.4 mg/L valine]. The medium was amended with no exogenous fatty acids (control), 100 μg perdeuterated pentadecanoic acid (C15:0 FA), or 100 μg perdeuterated octadecanoic acid (C18:0) from 10 mg/mL stock solutions in DMSO (addition of 100 μL the solvent alone did not affect growth). The perdeuterated fatty acids were purchased from CDN Isotopes and are completely deuterated [$CD_3(CD_2)_{13}COOH$ and $CD_3(CD_2)_{16}COOH$] with the sole exception of the carboxylic acid hydrogen (which exchanges too quickly in solution to retain a label). Cells were harvested in early stationary phase ($OD_{600} \approx 0.8$), washed twice, and frozen immediately. Samples were transesterified in the presence of a base catalyst (0.5 M NaOH in anhydrous methanol) at room temperature for 10 min (39). Free fatty acids are not transesterified under these basic conditions, which prevented the derivatization of any remaining exogenous perdeuterated free fatty acids not consumed by the microorganisms or removed during washing steps. The resulting FAMEs from all samples were extracted into hexane after addition of a quantification standard (10 μ g C25:0 FAME), and concentrated under a stream of N_2 at room temperature before analysis. All preparation, processing, and analysis of samples containing perdeuterated materials was performed in a separate laboratory to avoid any risk for cross-contamination of natural abundance or clinical isotope tracer experiments. Samples were analyzed on a Waters Micromass GCT Premier 6890N equipped with a Zebron-ZB-Wax column (29.5 m × 0.25 mm i.d., film thickness 0.25 μm) and PTV (programmable temperature vaporization) injector operated at a 10:1 split ratio, using He as a carrier gas at 15 mL/min. The GC oven was ramped at 2° C/min to 200° C, held for 1min, and ramped at 18° C/min to a final temperature of 250 °C (held for 7 min). Heavily deuterated fatty acids were detected as distinct peaks that eluted earlier than their respective natural abundance counterparts, and the degree of deuteration was determined from the mass shift of their molecular ions.

The data indicate that *S. aureus* is indeed capable of incorporating exogenous fatty acids *en bloc,* as can be seen from the presence of significant amounts of completely perdeuterated $C_{15:0}$ and $C_{18:0}$ in the intact polar lipids of the organism (Fig. S2). Additionally, it appears to be capable of elongating the exogenously provided free fatty acids by extension with 2 carbon units (acetyl-CoA), as witnessed by the presence of partly deuterated $C_{17:0}$ and $C_{19:0}$ when grown with perdeuterated $C_{15:0}$ (the mass spectrum reveals a completely deuterated C_{15} skeleton extended with undeuterated C_2/C_4) and partly deuterated $C_{20:0}$ when grown with perdeuterated $C_{18:0}$ (again, a completely deuterated C_{18} skeleton extended with undeuterated C_2). Curiously, none of these fatty acids are membrane components that *S. aureus* naturally produces in significant quantities (except some minor amounts of $C_{18:0}$), yet they constitute a significant portion of the intact polar lipid membrane fraction when provided exogenously. It is striking that the major, naturally occurring component that is altered the most in its abundance is the longer chain *a*-$C_{17:0}$ fatty acid, which is produced naturally by elongation of *a*-$C_{15:0}$. This suggests either that chain elongation of the exogenous fatty acids directly competes for substrate (acetyl-CoA) with elongation of a-$C_{15:0}$ to make a-$C_{17:0}$ FA or that a regulatory response of the organism compensates for the presence and effect of the longer-chain fatty acids on the physical properties of the membrane by reducing a-$C_{17:0}$ production.

The second observation, however, is that, unlike *P. aeruginosa*, *S. aureus* does not appear to partly break down the exogenous fatty acids and build them back up during fatty acid degradation (no partly deuterated fatty acids shorter than C_{17}/C_{20} could be detected in any analysis). For the normally dominant components of its membrane (methyl branched *a*-$C_{15:0}$ and *a*-$C_{17:0}$ fatty acids), this is consistent with the known biosynthetic pathway of anteiso methyl branched fatty acids, which are built from an

isoleucine primer in de novo fatty acid synthesis (55), and cannot be initiated from any partially degraded straight chain fatty acid by known biosynthetic mechanisms.

This indicates that *S. aureus*' methyl branched fatty acids (a-$C_{15:0}$ and a-$C_{17:0}$) measured in the lung environment are pure products of de novo synthesis. For this reason, we focus on these biomarkers for this study. It is important to note that, for fatty acids potentially elongated directly from exogenous precursors (e.g., $C_{18:0}$), the potential rate of fatty acid recycling must be considered carefully in any environment that experiences a heavy continuous influx of exogenous fatty acids from breakdown of organic matter. If the contribution of a precursor or component that can be incorporated *en bloc* is solely from other members of the same population, any isotopic spike still captures the activity of the population as a whole.

Testing for isotope label tolerance. Because heavy water is known to be toxic at high concentrations (18), we tested the susceptibility of *S. aureus* to ^2H_2O by growing the organism in SCFM with varying concentrations of ^2H_2O up to 35%. The growth experiment was performed at 37 °C in 96 well plates with four replicates per culture condition, and was inoculated from an overnight culture that had not previously experienced elevated levels of ^2H_2O. Plates were shaken continuously, and optical density (OD_{600nm}) was recorded every 5 min. The results (Fig. S3) show that there are no clear adverse effects of ^2H_2O doses as high as 35% on the growth of *S. aureus* in this medium. It is important to note, however, that the SCFM medium only approximates the nutritional environment of sputum and could fail to mimic other relevant chemical and structural features of sputum. To reduce the risk of the potentially toxic effects of high levels of ^2H_2O in sputum, we only used heavy water spikes well below the experimentally constrained 35%.

Data Processing for the Analysis of Clinical Samples. In this study, the isotopic enrichment of ^2H resulting from growth of *S. aureus* in the presence of ^2H spiked water is traced by measuring the isotopic composition of the nonexchangeable hydrogen bound in membrane fatty acids. The most basic equation relating isotopic enrichment to growth was introduced in Eq. **S5**. However, Eq. **S5** is based on the simplifying assumption that newly synthesized biomass directly reflects the isotopic composition of the heavy water tracer without taking into consideration additional effects such as the noninstantaneous penetration of the heavy water label into a clinical sample (consideration a), water hydrogen metabolism of the target organism (consideration b), and maintenance contributions to anabolic activity (consideration c). These effects and their magnitudes are outlined in the data processing roadmap in Fig. 2. The corresponding data corrections are derived in detail hereafter and are presented together with the data that we collected to constrain the individual parameters. In the context of fatty acid enrichment ($^2F^I_{fa_{new}} = {}^2F_{w_{spiked}}$), the starting equation (without corrections, labeled I) becomes

$$^2F_{fa}(t)^{\mathrm{I}} = {}^2F_{w_{spiked}} \cdot (1 - e^{-\mu \cdot t}) + {}^2F_{fa_{original}} \cdot e^{-\mu \cdot t}. \qquad \textbf{[S7]}$$

Accounting for label penetration into the sample. Water provides an excellent isotope tracer due to its rapid self-diffusivity, which is well-understood in aqueous solutions ($\sim 2.9 \times 10^{-5} cm^2 \cdot s^{-1}$ for H_2O at 35 °C, almost identical for $H_2{}^{18}O$, lower for fully tritiated water ^3H_2O at 0.81 to $1.02 \times 10^{-5} cm^2 \cdot s^{-1}$) (56), but more difficult to assess in the context of the irregularly shaped, highly viscous, biofilm-like sputum samples.

On long time scales (days to months), water diffusion would be negligible, but, due to the short incubation time scales required for quasi in situ experiments with expectorated sputum samples (~1 h), this effect can become relevant (i.e., sputum water cannot be assumed to adopt the spiked isotopic composition $^2F_{w_{spiked}}$ instantaneously). The lack of data and complexity of sputum poses difficulty in calculating the diffusion of the isotopic label into the sputum water ab initio. Here, we instead conducted several experiments with differently sized sputum samples (from ~0.5 g to 2.5g) to derive a simple empirical relationship of the form $1 - e^{-kt}$ and estimate the time-dependent isotopic composition of sputum water [$^2F_{w_{sputum}}(t)$] that allows a functional parametrization of the average isotopic composition that the microorganisms in the sputum experience over time. In these experiments, the equilibration of the hydrogen isotopic composition of water in the isotope labeling solution [$^2F_{w_{sputum}}(t)$] from exchange with water contained within the suspended sputum sample [$^2F_{w_{sputum}}(t)$] (mixed about 2:1 wt/wt) was tracked over time, as illustrated in Fig. S4*A*. The hydrogen isotope composition of both end-member pools was described as exchanging toward the equilibrium isotope composition $^2F_{w_{eq}}$ of the fully exchanged combined water pool with rate constant k,

$$^2F_{w_{sln}}(t) = {}^2F_{w_{eq}} + \left({}^2F_{w_{spike}} - {}^2F_{w_{eq}}\right) \cdot e^{-k \cdot t} \qquad \textbf{[S8]}$$

$$^2F_{w_{sputum}}(t) = {}^2F_{w_{eq}} + \left({}^2F_{w_{nat}} - {}^2F_{w_{eq}}\right) \cdot e^{-k \cdot t} \qquad \textbf{[S9]}$$

where $^2F_{w_{spike}}$ is the hydrogen isotope composition of the spiked isotope labeling solution (i.e., $^2F_{w_{sln}}$ at t_0), and $^2F_{w_{nat}}$ is the natural isotope composition of water contained within the sputum sample (i.e., $^2F_{w_{sputum}}$ at t_0). The data in Fig. S4*A* are fitted to Eq. **S8** (fit of Eqs. **S8** and **S9** illustrated in dashed and dotted lines, respectively), to derive a measure of k for each sample.

Fig. S4*B* illustrates the derived values of k, which show a relationship with the sample weight as expected, and provides a model to estimate k for samples of differing weights. As sputum samples become larger, it takes water from the isotopic labeling solution longer to exchange with water in the sputum sample. To minimize the effect of this noninstantaneous water exchange, we aimed for an ideal clinical sample size of ~0.8 g. Fig. S4 *C* and *D* illustrates the extent of this effect for a typical clinical sample.

For each isotopically labeled clinical sample, the hydrogen isotope composition of water in the labeling solution [$^2F_{w_{sputum}}(t)$] was measured in the residual solution at the conclusion of the experiment (at time t_{inc}), and the corresponding equilibrium isotopic composition between labeling solution and sample water ($^2F_{w_{eq}}$) was calculated using the estimated value of k for the given sample weight,

$$^2F_{w_{eq}} = \frac{{}^2F_{w_{sputum}}(t_{inc}) - {}^2F_{w_{spike}} \cdot e^{-k \cdot t_{inc}}}{1 - e^{-k \cdot t_{inc}}}. \qquad \textbf{[S10]}$$

Based on these parameters, we can use Eq. **S9** to model the time course of the sputum water isotopic composition that the microbial population experiences over the entire incubation time interval.

Assuming that newly synthesized fatty acids directly reflect the isotopic composition of the source water for now (see correction for this in *Accounting for water hydrogen metabolism of the target organism*), we can use $F_{fa_{new}}(t)^{\mathrm{II}} = F_{w_{sputum}}(t)$ to solve the original isotope mass balance (Eq. **S4**) from integral form, essentially adding a corrective term for the noninstantaneous water exchange to the starting equation [Eq. **S7**/$^2F_{fa}(t)^{\mathrm{I}}$],

$$\begin{aligned} {}^2F_{fa}(t)^{\mathrm{II}} &= \left[\int_0^t F_{fa_{new}}(t)^{\mathrm{II}} \cdot \mu \cdot e^{-\mu t} \cdot dt\right] + {}^2F_{fa_{original}} \cdot e^{-\mu t} \\ &= {}^2F_{fa}(t)^{\mathrm{I}} - \left({}^2F_{w_{eq}} - {}^2F_{w_{nat}}\right) \cdot \frac{\mu}{\mu + k} \cdot \left(1 - e^{-(\mu + k) \cdot t}\right). \end{aligned} \qquad \textbf{[S11]}$$

Accounting for water hydrogen metabolism of the target organism. During the biosynthesis of fatty acids, the resulting macromolecules

generally follow the isotopic composition of the source water the organism is growing in. However, because of isotopic fractionation during biosynthesis and because not all H atoms are derived from water, this is not a 1:1 relationship. The isotopic composition of newly synthesized fatty acids can be considered in terms of the combination of the mole fraction of water derived hydrogen (x_w) and associated net hydrogen isotope fraction ($\alpha_{fa/w}$), and substrate-derived hydrogen ($x_w - 1$) including metabolic water (57) with average substrate isotopic composition ($^2F_{sub}$) and associated net isotope fractionation ($\alpha_{fa/s}$) (21),

$$^2F_{fa_{new}}(t) = x_w \cdot \alpha_{fa/w} \cdot {}^2F_{w_{spiked}} + (1 - x_w) \cdot \alpha_{fa/s} \cdot {}^2F_{sub}. \quad \textbf{[S12]}$$

Isotopic fractionation factors are defined with respect to isotope ratios ($\alpha_{b/a} = R_b/R_a$); see *Error from using fractionation factors in exact mass balance calculations* for details on the use of fractionation factors with fractional abundances.

For growth under similar conditions (medium, temperature, etc.), the physiological parameters of hydrogen assimilation (x_w, $\alpha_{fa/w}$, $\alpha_{fa/s}$) are assumed to be comparable. The appropriate value of the combined water hydrogen assimilation constant $a_w = x_w \cdot \alpha_{fa/w}$ for *S. aureus* growing in clinical samples was determined in SCFM (20) following the approach of ref. 21. Briefly, *S. aureus* was grown in batch culture experiments with four different water isotopic compositions, and a_w was determined for all major membrane fatty acids from the slopes of $^2F_{fa}$ vs. $^2F_{water}$ (Fig. S5). For calculations involving bulk fatty acid hydrogen isotope compositions, an average value for a_w (average $a_w = 0.41$) was determined from all fatty acids' a_w values weighted by the relative abundances of the individual fatty acids. The substrate-dependent contribution to fatty acid hydrogen was determined from the fatty acids' and sputum water's natural isotopic compositions in clinical samples,

$$(1 - x_w) \cdot \alpha_{fa/s} \cdot {}^2F_{sub} = {}^2F_{fa_{nat}} - a_w \cdot {}^2F_{w_{nat}}.$$

Combing these parameters with Eq. **S9** (the time-dependent spiked water exchange), the expression for the isotopic composition of newly synthesized fatty acids (Eq. **S12**) becomes

$$\begin{aligned} {}^2F_{fa_{new}}(t)^{\mathrm{III}} &= a_w \cdot \left({}^2F_{w_{sputum}}(t) - {}^2F_{w_{nat}}\right) + {}^2F_{fa_{original}} \\ &= a_w \cdot \left({}^2F_{w_{eq}} - {}^2F_{w_{nat}}\right) \cdot \left(1 - e^{-k \cdot t}\right) + {}^2F_{fa_{original}}. \end{aligned} \quad \textbf{[S13]}$$

Finally, this equation can be used to once again solve the original isotope mass balance (Eq. **S4**) from integral form, adding a second term to Eq. **S17** ($^2F_{fa}(t)^{\mathrm{II}}$),

$$\begin{aligned} {}^2F_{fa}(t)^{\mathrm{III}} &= \left[\int_0^t {}^2F_{fa_{new}}(t)^{\mathrm{III}} \cdot \mu \cdot e^{-\mu t} \cdot dt\right] + {}^2F_{fa_{original}} \cdot e^{-\mu t} \\ &= a_w \left({}^2F_{fa}(t)^{\mathrm{II}} - {}^2F_{w_{nat}}\left(1 - e^{-\mu t}\right)\right) \\ &\quad + {}^2F_{fa_{original}} \cdot \left(1 - a_w \cdot e^{-\mu t}\right). \end{aligned} \quad \textbf{[S14]}$$

Accounting for maintenance contribution to anabolic activity. Because our approach captures the overall anabolic activity including both the specific growth rate μ (which signifies true cellular replication), and the maintenance turnover rate ω (which describes biosynthesis in excess of growth to compensate for degradation and material turnover), quantifying growth (μ) requires constraints on the maintenance contribution.

S. aureus MN8 was thus grown continuously in a chemostat system (Sartorius Biostat QPlus) in SCFM amended with 500 μ L/L Antifoam 204 (A6426; Sigma Aldrich) at 37 °C with agitation. The chemostat vessel with ~550 mL working volume was inoculated from a single colony pregrown in the same medium, and continuous supply of medium was started upon reaching early stationary phase and maintained at a flow rate equivalent to a generation time of 4.9 d (0.14 divisions per day). Overflow from the vessel was continuously removed to maintain a fixed volume, and the exact dilution rate was confirmed gravimetrically from the total vessel content and medium flow rate. Redox potential, pH, and dissolved oxygen were monitored continuously, and optical density was measured in aliquots withdrawn aseptically from vessel overflow. After the monitored physiological parameters reached steady state (after approximately six generations), the chemostat vessel was spiked with 2 mL 70% ^2H_2O, and ^2H incorporation into fatty acids was monitored over time.

At steady state, the growth rate of the culture (μ) must equal the known rate of dilution (d, corresponding to 4.9 d doubling time), which leaves the fatty acid maintenance rate ω as the only unconstrained parameter in this system. Unlike in clinical samples, the isotopic composition of the medium water decreases over time after the initial spike due to dilution of the tracer from the continuous supply of fresh medium (to maintain steady-state growth conditions). The water isotopic composition of the enriched medium is thus a function of the initial composition of the spiked medium ($^2F_{w_{spiked}}$), and the dilution with fresh medium of original water isotopic composition ($^2F_{w_{nat}}$) at dilution rate d,

$${}^2F_w(t) = {}^2F_{w_{spiked}} \cdot e^{-d \cdot t} + {}^2F_{w_{nat}}\left(1 - e^{-d \cdot t}\right). \quad \textbf{[S15]}$$

Using this equation with Eq. **S13** [for $^2F_{fa_{new}}(t)$] to solve the original isotope mass balance (Eq. **S4**) from integral form but with $\omega > 0$ yields the following solution for the chemostat system (CH):

$$\begin{aligned} \text{Chemostat}: {}^2F_{fa}(t) &= a_w \cdot \left({}^2F_{w_{spiked}} - {}^2F_{w_{nat}}\right) \\ &\quad \cdot \left[\frac{\mu + \omega}{\mu + \omega + d} \cdot \left(1 - e^{-(\mu + \omega + d) \cdot t}\right)\right] \\ &\quad + {}^2F_{fa_{original}}. \end{aligned} \quad \textbf{[S16]}$$

By fitting the time-dependent fatty acid enrichment from this isotope labeling experiment (Fig. S6) to Eq. **S16**, ω was calculated to amount to 56% of the growth rate ($\omega/\mu = 0.56$). Although maintenance turnover rates are sometimes considered to reflect a constant absolute rate of repair or basic energy requirement, this rate is likely variable, and depends on the actual population growth rate as discussed by ref. 58. In this study, we assumed that the maintenance rate scales with the growth rate and approximated the minimum fatty acid maintenance turnover rate for each clinical sample from the relative maintenance rate of 56% measured in our continuous culture experiment. If the chemical environment within the sputum requires higher relative rates of fatty acid maintenance/repair than the chemically stable environment of the chemostat, the clinical growth rates would be even lower than currently estimated (Fig. 3).

Final population growth rate calculations. Finally, incorporating the equations and parameters for all three corrections—non-instantaneous water exchange (consideration a, Eq. **S9**), the hydrogen metabolism of *S. aureus* (consideration b, Eq. **S13**), and the maintenance turnover (consideration c, ω)—into the integral form of Eq. **S4** yields the following equation for

linking fatty acid hydrogen isotope composition to growth rates in the clinical samples:

$$\begin{aligned}\text{Clinical}: {}^2F_{fa}(t) = &\left[\int_0^t F_{fa_{new}}(t)^{\text{III}} \cdot (\mu+\omega) \cdot e^{-(\mu+\omega)t} \cdot dt\right] \\ &+ {}^2F_{fa_{original}} \cdot e^{-(\mu+\omega)t} = a_w \cdot \left({}^2F_{w_{eq}} - {}^2F_{w_{nat}}\right) \\ &\cdot \left[1 - e^{-(\mu+\omega)\cdot t} - \frac{\mu+\omega}{\mu+\omega+k} \cdot \left(1 - e^{-(\mu+\omega+k)\cdot t}\right)\right] \\ &+ {}^2F_{fa_{original}}. \end{aligned} \quad \textbf{[S17]}$$

All microbial growth rates were estimated by numerically fitting the clinical data to this equation. The turnover rate ω was constrained with data from continuous culture experiments with *S. aureus* as described above. In addition to growth rate estimates from the isotopic enrichment of individual key fatty acids of *S. aureus* (a-$C_{15:0}$ and a-$C_{17:0}$), the overall growth rate of *S. aureus* populations was calculated from the average bulk membrane isotopic composition ${}^2F_{SA} = f \cdot {}^2F_{a15} + (1-f) \cdot {}^2F_{a17}$ with relative total fatty acid abundance ratio $f = A_{a15}/(A_{a15} + A_{a17})$.

Additional considerations for single-cell analysis. The use of plastic thin sections for NanoSIMS analysis allowed accurate targeting and identification of individual microorganisms despite the small size of the pathogens, and the structurally complex nature of the sputum samples. The resin used in this study, Technovit 8100, polymerizes at cold temperatures (~4 °C), precluding the need for extended exposure to relatively high heat (and the associated risk for structural changes). The structural support lent by the plastic matrix provided thin sections with a smooth surface that enabled high spatial resolution during NanoSIMS analysis due to the lack of topological features (27). However, as an acryl plastic (a combination of methyl methacrylate and glycol methacrylate), the Technovit resin contributed significant amounts of isotopically circumnatural carbon and hydrogen that dilute the isotopic signal from enriched cells. To correct for this effect, we calibrated both free and plastic-embedded single cell measurements against bacterial isotope standards in ref. 27.

Raw data from all acquired ion images were processed using the open-source MATLAB plugin Look@NanoSIMS (59). Ion images from multiple frames were corrected for dead time and QSA (quasi-simultaneous arrivals) effect and aligned, and the corresponding microscopy images were warped onto the $^{14}N^{12}C^-$ ion image using functionality provided by Look@NanoSIMS. Discrete regions of interest were hand-drawn around individual microbes based on the $^{14}N^{12}C^-$ ion image and the FISH+DAPI images. Fractional abundances of single cell analyses were calculated directly from raw ion counts and converted to bulk membrane equivalents using the reported calibration for hydrogen isotope measurements in embedded *S. aureus* cells (27). Single-cell growth rates were calculated using Eq. **S17** after converting the thin section NanoSIMS measurements to their corresponding bulk membrane enrichments. Based on the findings of Musat et al. (60) that stationary phase cells do not experience significant isotope label dilution from mono FISH treatment, we considered this direct application of the reported calibration (which does not include FISH treatment) to be most appropriate given the relatively low single-cell growth rates measured throughout the samples in this study.

Uncertainty Assessment. Here, we discuss the various sources of uncertainty introduced by analytical constraints and mathematical approximations that contribute to the uncertainty estimates for the growth rates presented in this study. Fig. S7 summarizes the sensitivity of the growth rate measurement to the uncertainty in key parameters.

Error from using fractionation factors in exact mass balance calculations. Exact mass balance calculations that use fractional abundances F, instead of δ-values or isotope ratios R, are important in isotope labeling experiments due to the large error introduced by approximating mass balance at higher isotopic enrichments in δ-value space. However, for biosynthetic processes that can cause significant isotopic fractionation, exact mass balance calculations require an approximation regarding the use of fractionation factors. An isotope fractionation factor between two pools a and b is usually reported/known in terms of the ratio of isotope ratios between the two pools, $\alpha_{b/a} = R_b/R_a$. In the relevant case for this study, i.e., the biosynthetic incorporation of water hydrogen into fatty acids discussed in *Materials and Methods*, the formulation of ${}^2F = x_w \cdot \alpha_{fa/w} \cdot {}^2F_{w_{sputum}} = a_w \cdot {}^2F_{w_{sputum}}$ is thus only an approximation of the exact calculation

$$\begin{aligned}{}^2F &= x_w \cdot \frac{\frac{\alpha_{fa/w} \cdot {}^2F_{w_{sputum}}}{1 - {}^2F_{w_{sputum}}}}{1 + \left(\frac{\alpha_{fa/w} \cdot {}^2F_{w_{sputum}}}{1 - {}^2F_{w_{sputum}}}\right)} \\ &= x_w \cdot \left[\frac{\alpha_{fa/w}}{1 + (\alpha_{fa/w} - 1) \cdot {}^2F_{w_{sputum}}}\right] \cdot {}^2F_{w_{sputum}} \\ &= a_{exact} \cdot {}^2F_{w_{sputum}}. \end{aligned} \quad \textbf{[S18]}$$

The relative error that this approximation introduces into the water assimilation constant a_w can be calculated as follows:

$$\begin{aligned}\frac{u_a}{a_w} &= \frac{a_w - a_{exact}}{a_w} \\ &= \frac{x_w \cdot \alpha_{fa/w} - x_w \cdot \frac{\alpha_{fa/w}}{1 + (\alpha_{fa/w} - 1) \cdot {}^2F_{w_{sputum}}}}{x_w \cdot \alpha_{fa/w}} \\ &= \frac{(\alpha_{fa/w} - 1) \cdot {}^2F_{w_{sputum}}}{1 + (\alpha_{fa/w} - 1) \cdot {}^2F_{w_{sputum}}}. \end{aligned} \quad \textbf{[S19]}$$

Although the combined assimilation constant $a_w = x_w \cdot \alpha_{fa/w}$ can be measured experimentally (*Materials and Methods*), the two individual parameters that describe the assimilation of hydrogen from water, i.e., the fraction x_w of fatty acid hydrogen derived from water, and the isotope fractionation $\alpha_{fa/w}$ associated with this biosynthetic pathway, cannot be experimentally separated for heterotrophic organisms. With current experimental approaches, the system is underconstrained. This limits the potential use of the exact formula above, which requires separate knowledge of x_w and $\alpha_{fa/w}$. However, ref. 21 estimated the range of possible values for $\alpha_{fa/w}$ for heterotrophic growth in complex media to fall between 0.8 (fractionation by −200‰) and 1.15 (+150‰). Based on these bounding estimates, we were able to constrain the error introduced by the approximation $(a_w \cdot {}^2F_{w_{sputum}})$ for each clinical sample using Eq. **S19**. This source of uncertainty (typically $1 - 4\% \cdot a_w$) was taken into consideration in all growth rate calculations in addition to the experimentally determined confidence interval for a_w.

Error propagation for analytical uncertainty. The uncertainty in individual FAME measurements u_{FAME} is constrained by the combined effects of the analytical uncertainty (sample SD s_{FAME}) and the maximal potential offset caused by hydrogen isotope memory effects (61) of 4% the difference in the isotope value to the preceding methane reference peaks. This provides a conservative upper bound on the error estimate. In reality, analysis

of methane reference standards that follow analytical peaks suggests memory effects to be much lower (~0.2% instead of 4%).

$$\begin{aligned}&\text{upper bound}: u_{FAME} = s_{FAME} + 0.04 \cdot (F_{FAME} - F_{CH_4})\\ &\text{lower bound}: u_{FAME} = s_{FAME}.\end{aligned} \quad \textbf{[S20]}$$

The FAME uncertainty is propagated to the uncertainty in the fatty acids themselves, u_{FA}, by SE propagation of the derivatization correction equation (assuming that the error in the FAME and MeOH measurements are uncorrelated).

$$F_{FA} = \frac{\#\mathrm{H}_{FA} + 3}{\#\mathrm{H}_{FA}} \cdot F_{FAME} - \frac{3}{\#\mathrm{H}_{FA}} \cdot F_{MeOH} \quad \textbf{[S21]}$$

$$u_{FA} = \sqrt{\left(\frac{\#\mathrm{H}_{FA} + 3}{\#\mathrm{H}_{FA}} \cdot u_{FAME}\right)^2 + \left(\frac{3}{\#\mathrm{H}_{FA}} \cdot u_{MeOH}\right)^2}. \quad \textbf{[S22]}$$

During the calculation of *S. aureus* average isotopic composition ${}^2F_{SA}$ from the *a*-C15:0 and *a*-C17:0 fatty acids and their relative abundance $f = A_{a15}/(A_{a15} + A_{a17})$, the uncertainties ($u_{a15}$, u_{a17}, and u_f) are propagated as well by SE propagation, taking into account the covariance between the quantities ($\mathrm{cov}_{a15\&a17}$, $\mathrm{cov}_{a15\&f}$, and $\mathrm{cov}_{a17\&f}$), which are estimated from the data.

$$F_{SA} = f \cdot F_{a15} + (1 - f) \cdot F_{a17}. \quad \textbf{[S23]}$$

The uncertainty in the isotopic composition of spiked sputum water ($F_{w_{eq}}$) discussed in *Materials and Methods* was calculated similarly by SE propagation from uncertainties in the water exchange rate constant k, sample incubation time, and water isotopic compositions ($F_{w_{sln}}$ and $F_{w_{spike}}$). Because Eq. **S17** does not have an analytical solution for the growth rate μ, the upper and lower error bounds (μ_{min} and μ_{max}) were estimated from the maximal combined uncertainties of all key parameters that offset the growth rate positively and negatively. The sensitivities to the different errors are illustrated graphically in Fig. S7. Error bars in Fig. 3 indicate this conservative error estimate for the calculated bulk population growth rates.

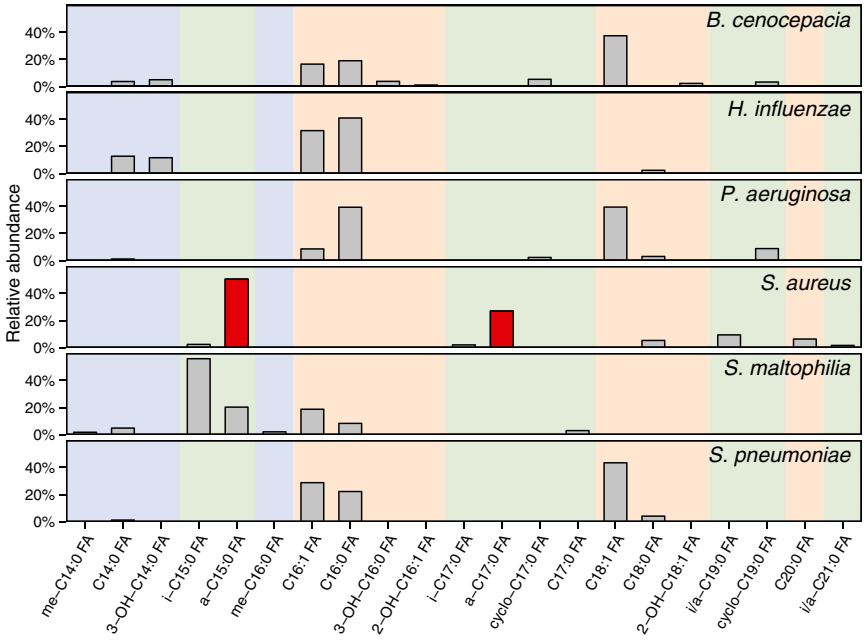

Fig. S1. *S. aureus* produces characteristic fatty acids distinct from host and competitors. Different pathogens have different fatty acid fingerprints that provide species-specific targets for growth rate measurements. However, only a subset is exclusively microbial (green shaded) or usually microbial (blue shaded), with several major fatty acids unsuitable for targeted analysis because they are also produced by host cells (orange shaded). We focused on *S. aureus* and targeted its most characteristic fatty acids (highlighted in red): *a*-$C_{15:0}$ and *a*-$C_{17:0}$, the anteiso methyl branched C_{14} and C_{16} saturated fatty acids.

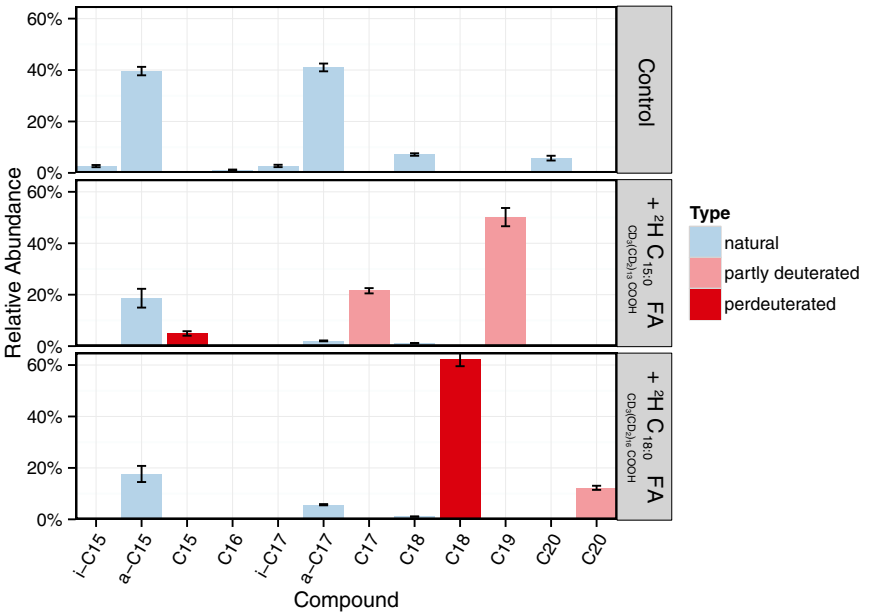

Fig. S2. *S. aureus* does not recycle exogenous fatty acids for the synthesis of methyl branched (*a*-$C_{15:0}$, *a*-$C_{17:0}$) fatty acids. We investigated whether *S. aureus* is capable of recycling exogenous fatty acids it might encounter in the lung environment to derive the biomarkers (*a*-$C_{15:0}$ and *a*-$C_{17:0}$) targeted in this study. The lack of fatty acid recycling is a critical aspect for this quantitative approach; if organisms build the targeted lipids from exogenous fatty acids, the amount of ^2H incorporated from heavy water would be greatly reduced and therefore underestimate population growth rates. To test this, two perdeuterated precursor fatty acids (the naturally abundant octadecanoic acid and the microbially produced pentadecanoic acid, both entirely ^2H-substituted in the hydrocarbon tail) were provided as an exogenous source of free fatty acids to test for recycling by *S. aureus* (*Bottom* and *Middle*, respectively). Although *S. aureus* is capable of elongating the exogenous fatty acids to produce longer-chain derivatives, it does not appear to partly break down the exogenous fatty acids and build them back up, unlike *P. aeruginosa* (no partly deuterated fatty acids shorter than C_{17}/C_{20} could be detected in any analysis). This indicates that *S. aureus*' methyl branched fatty acids (*a*-$C_{15:0}$ and *a*-$C_{17:0}$) measured in the lung environment are products of de novo synthesis and can be targeted for growth rate measurements.

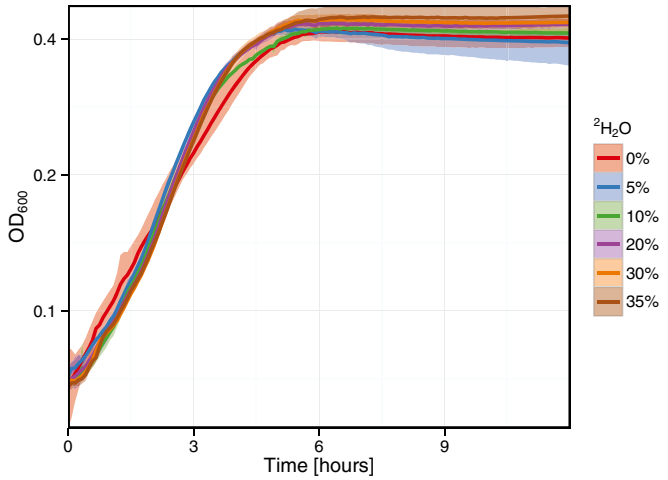

Fig. S3. *S. aureus* has a high tolerance for ^2H_2O in synthetic cystic fibrosis medium. We investigated the toxicity effects of increasing concentrations of ^2H_2O on *S. aureus*. This figure shows the semilog growth curves of *S. aureus* in the presence of varying amounts of ^2H_2O. Lines represent averages of at least four biological replicates; shaded area represents the maximal range of ODs in each condition.

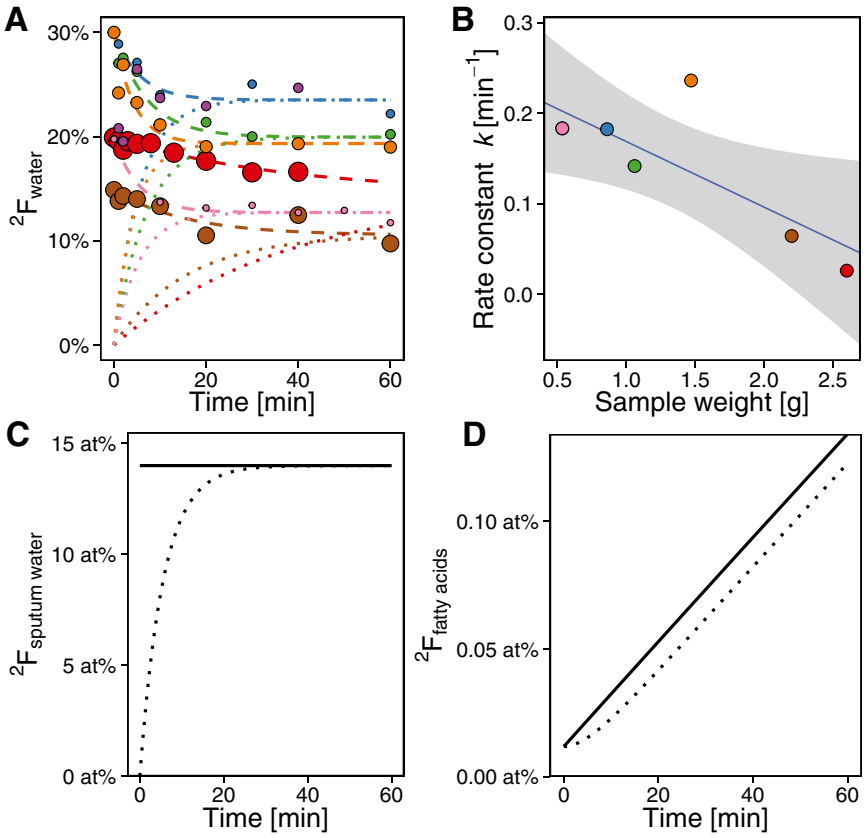

Fig. S4. Parameterization of noninstantaneous water exchange. The isotopic composition of newly synthesized fatty acids after administration of the isotopic water spike depends on the isotopic composition of sputum water in the clinical samples. For this study, we conducted experiments with differently sized sputum samples (0.5–2.5 g) to derive an empirical relationship for the water equilibration time that would allow a functional parameterization of the average isotopic composition microorganisms experience in the sputum over time. (*A*) The measurements of saline solution around sputum over time: ^2F decreases as the label is exchanged into the sputum. Experiments are grouped by color, symbol sizes reflect sample weights, and dashed/dotted lines illustrate the best-fit equilibration curves for the heavy water spike/sputum water. (*B*) The expected sample weight dependence of the equilibration rate constant; i.e., as sputum samples become larger, it takes water from the isotopic labeling solution longer to exchange with water in the sputum sample. (*C* and *D*) The extent of the noninstantaneous water exchange effect for an average clinical sample. The solid lines show the modeled isotopic composition of the sputum water (*C*) and resulting fatty acid enrichment (*D*) if water exchange between the labeling solution and the sample were instantaneous. The dotted lines show the same metrics for a typical clinical sample (average weight of 0.86 g), based on the empirically derived water exchange model used in this study. The fatty acid enrichment for both conditions is modeled using the average growth rate measured in clinical sample.

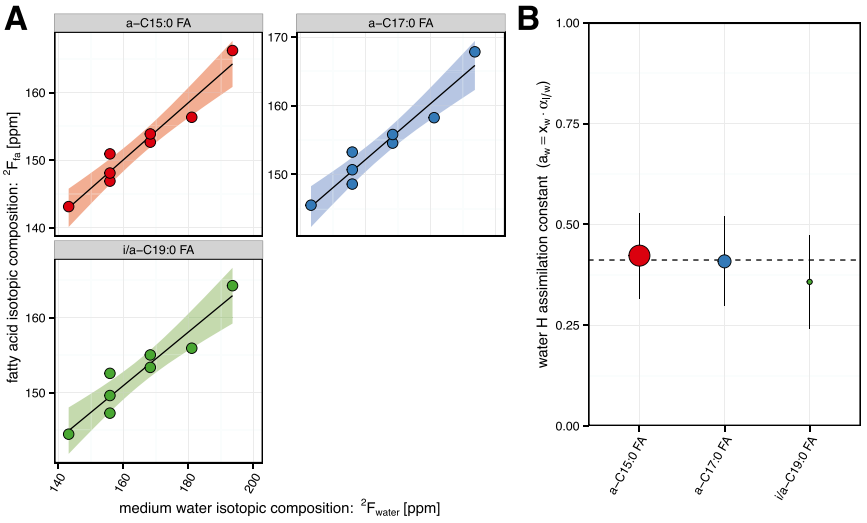

C

Compound	% Membrane	water H assimilation constant (a_w)	R^2
a-C15:0 FA	51.2	0.42 ± 0.11	0.941
a-C17:0 FA	29.6	0.41 ± 0.11	0.931
i/a-C19:0 FA	8.5	0.36 ± 0.12	0.905

Fig. S5. Physiological parameters of water hydrogen assimilation. The isotopic composition of newly synthesized fatty acids after administration of the isotopic water spike depends partly on the physiology of hydrogen assimilation from water. The value of the water hydrogen assimilation constant (a_w) for *S. aureus* was determined from the slopes of the hydrogen isotope compositions of individual fatty acids ($^2F_{fa}$) vs. medium water hydrogen isotope composition ($^2F_{water}$) in cultures grown in synthetic cystic fibrosis medium with variable water isotope compositions. (*A*) The regression lines for individual fatty acids with 95% confidence bands. (*B*) A summary of the water hydrogen assimilation constants (a_w) derived for individual fatty acids from regression analysis of *A*, and (*C*) their numerical values. The size of the symbols in *B* indicates the relative membrane abundance of the individual fatty acids. Error bars indicate 95% confidence intervals of the coefficients from the linear regression fit. The dashed horizontal line illustrates the average value for a_w (0.41), determined from all fatty acids' a_w values weighted by the relative abundances of the individual fatty acids.

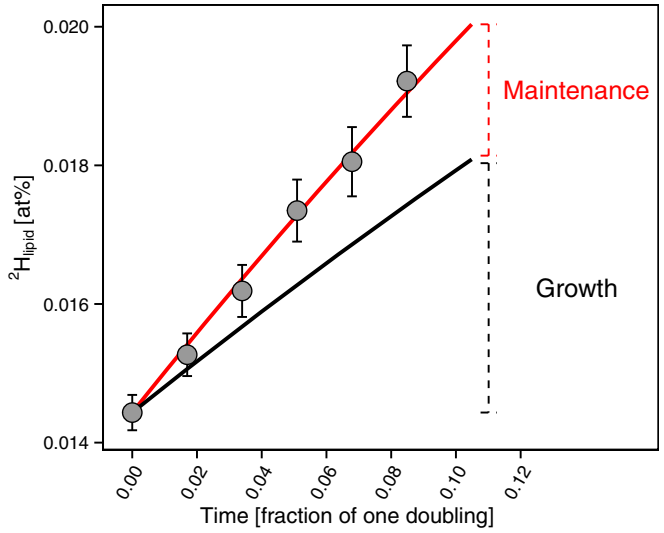

Fig. S6. Chemostat constraints on maintenance vs. growth. Symbols show the time-dependent isotopic enrichment of *S. aureus* membrane fatty acids (weighted average isotopic composition of the different membrane components). The *x* axis records the time after spiking a steady-state culture of *S. aureus* growing at a controlled growth rate of 0.14 divisions per day (doubling time of ~4.9 d) with heavy water. The relative fatty acid maintenance turnover rate was calculated from ^2H uptake in excess of growth and was determined to amount to 56% of the growth rate.

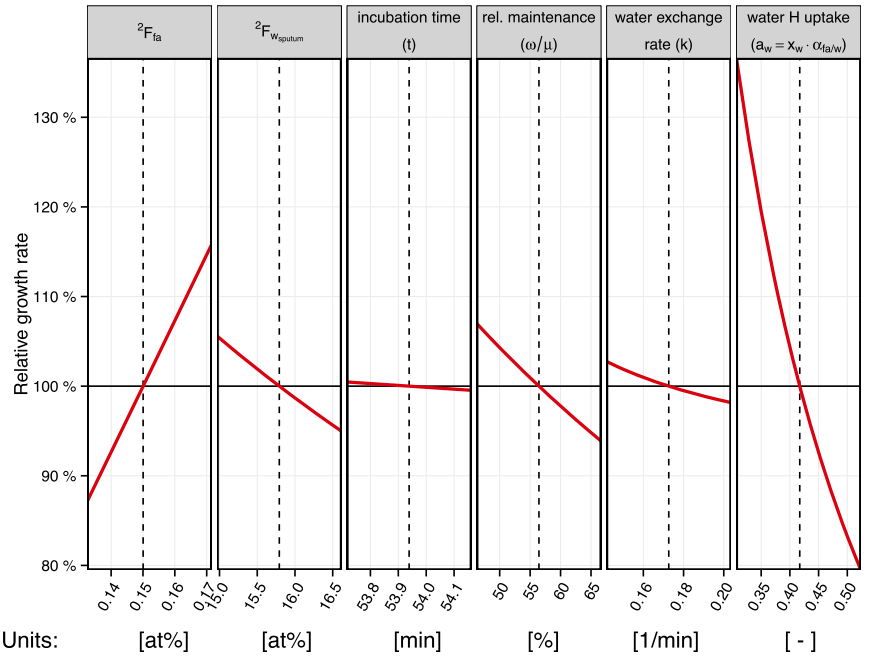

Fig. S7. Sensitivity of growth rate calculations to parameter uncertainty. Various sources of uncertainty introduced by analytical constraints and mathematical approximations contribute to the uncertainty estimates for the growth rates presented in this study. This figure provides a visual summary of the sensitivities to the different error sources. Dashed vertical lines indicate the average value of each parameter for the clinical samples (fatty acid isotopic composition, spiked sputum water isotopic composition, incubation time, fatty acid maintenance turnover, water exchange rate, and water hydrogen assimilation constant). The sensitivities of the growth rate estimates to the uncertainty ranges considered for each parameter are illustrated in red. Because the growth equation in this system (Eq. **S17**) does not have an analytical solution for the growth rate, the upper and lower error bounds presented in Fig. 3 were estimated from the maximal combined uncertainties of all key parameters that offset the growth rate positively and negatively.

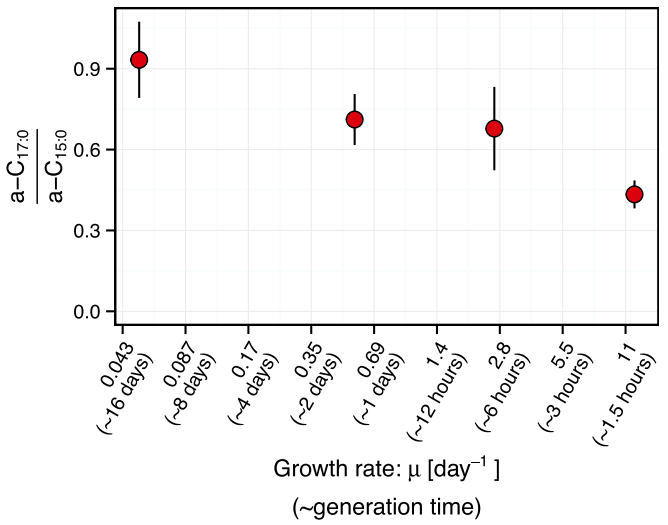

Fig. S8. The membrane composition of *S. aureus* is growth rate-dependent. Lipid profile data from laboratory experiments at different growth rates suggest that slower growing populations of *S. aureus* shift their membrane composition to a higher *a*-$C_{17:0}$ ratio (average *a*-$C_{17:0}$ to *a*-$C_{15:0}$ fatty acid ratio of *S. aureus* membranes are plotted as a function of growth rate; growth rate is plotted on a log scale for clarity). This could explain the observation in clinical samples that *a*-$C_{15:0}$ systematically incorporates more isotope tracer than *a*-$C_{17:0}$, potentially reflecting underlying heterogeneity in the microbial population with slower-growing cells producing *a*-$C_{17:0}$ preferentially and faster-growing cells producing *a*-$C_{15:0}$. Data are from Kopf et al. (27).

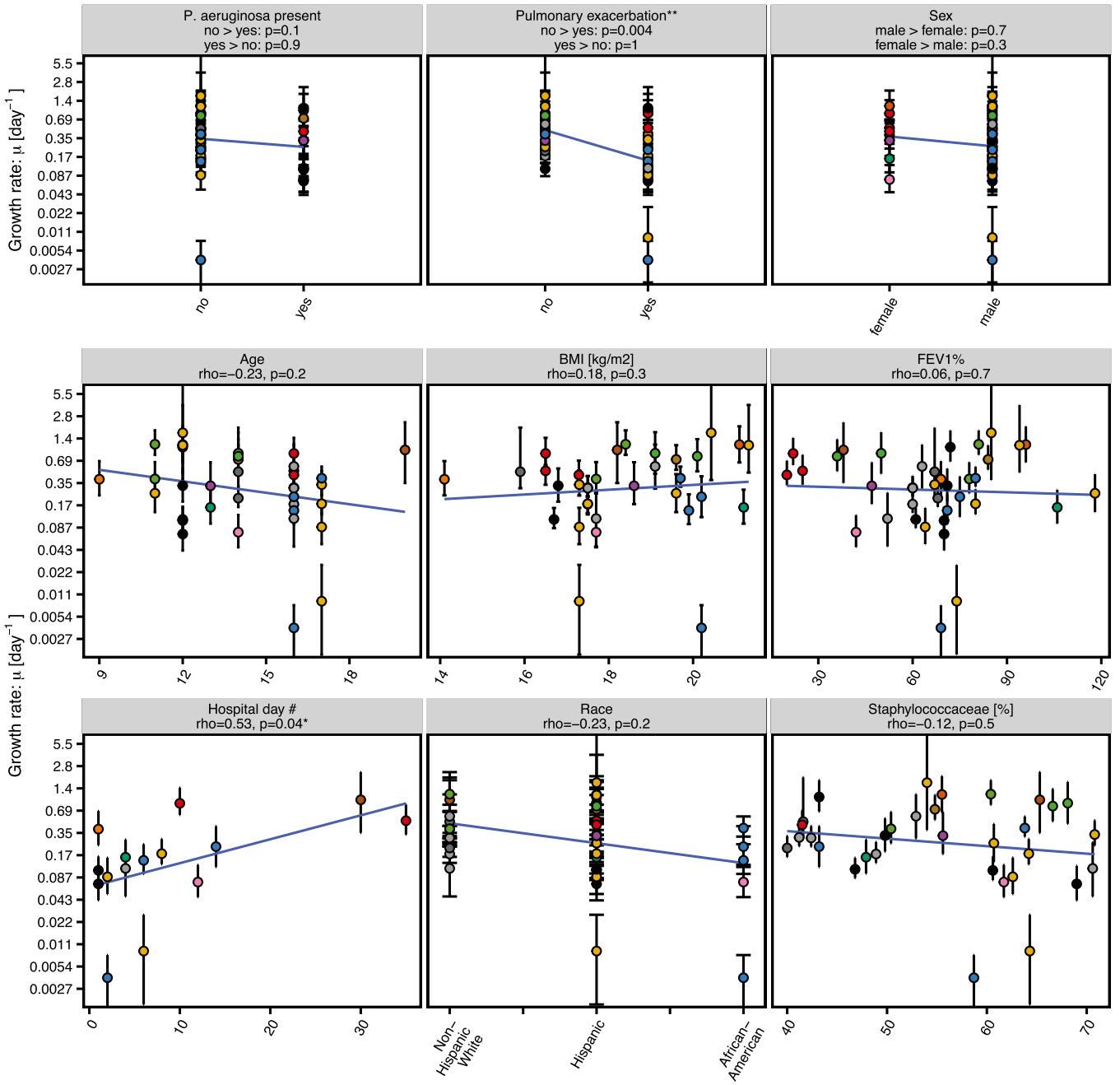

Fig. S9. *S. aureus* growth rates are correlated with few clinical parameters. This figure expands on correlations with clinical parameters discussed in *Correlation with Clinical Parameters* (Table 1) and illustrates the correlation between the clinical parameters and the measured bulk growth rates for *S. aureus*. (*Top*) Each panel denotes a different binary parameter with the respective *P* values of the MWW test for the alternative hypotheses indicated in the header. (*Middle* and *Bottom*) Each panel shows the respective Spearman correlation coefficient and *P* value for the correlation. The different colors indicate samples from different patients in the study. All growth rates (*y* axis) are plotted on a log scale for clarity. Not all clinical information was available for all data points (see Table S1 for data).

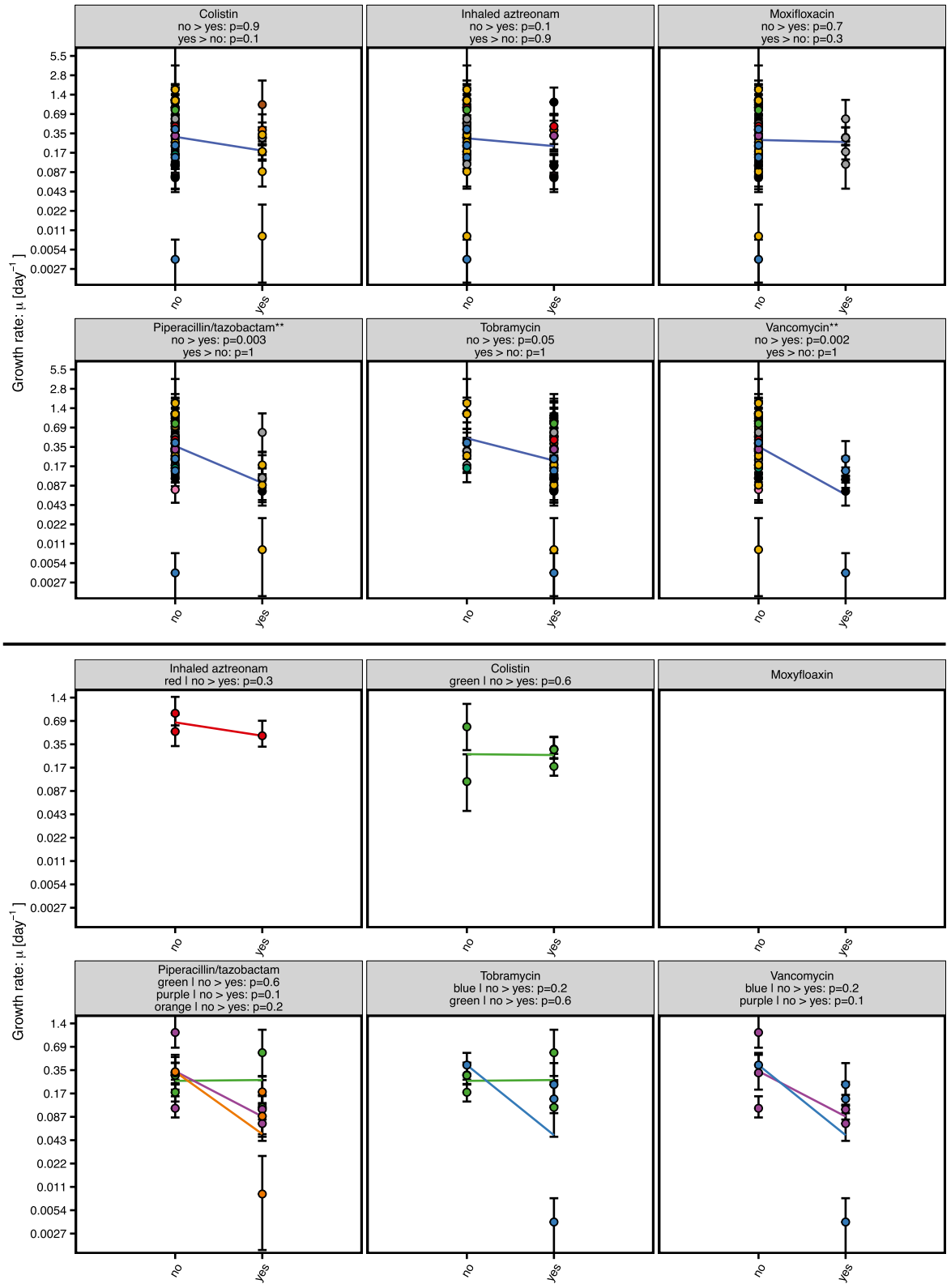

Fig. S10. *S. aureus* growth rates are correlated with specific antibiotic treatments, but more longitudinal data are required at the patient level. This figure expands on correlations with clinical parameters discussed in *Correlation with Clinical Parameters* (Table 1) and illustrates the correlation between antibiotic treatments and the measured bulk growth rates for *S. aureus*. (*Top* and *Upper Middle*) Each panel in the denotes a different antibiotic with the respective *P* values of the MWW test for the alternative hypotheses indicated in the header. Only antibiotics with at least five samples in each category (yes/no) are shown. (*Lower Middle* and *Bottom*) Each panel in the shows the same data only for patients with data in both categories (yes/no) and respective statistical tests broken down on a per-patient basis. Patients are distinguished by color. All growth rates (*y* axis) are plotted on a log scale for clarity. Not all clinical information was available for all data points (see Table S1 for data).

Table S1. Patient and treatment information, health indicators, microbial community, and growth rates

Patient	Age	Sex	Race	BMI, kg/m^2	FEV1%	Pulmonary exacerbation	Hospital day no.	Active antibiotics*	*P. aeruginosa* present	*Staphylococcaceae*, %	Type	*S. aureus* clinical culture antibiotic resistance (R)/ susceptability (S)†	*Xanthomonadaceae*	Incubation time, min	Sample weight, g	$^2F_{w_{eq}}$, atom%	$^2F_{fa}$, atom%	*S. aureus* growth rate, 1/d
1	16	male	Non-Hispanic White	17.5	60	no	n/a	COL, ETH, MOX	n/a	41.2	MSSA	n/a	4.3%	61	0.7	12.3	0.105	0.3
1	16	male	Non-Hispanic White	17.5	60	no	n/a	COL, ETH, MOX	n/a	42.4	MSSA	n/a	5.1%	61	0.9	14.1	0.116	0.3
1	16	male	Non-Hispanic White	17.5	60	no	n/a	COL, ETH, MOX	n/a	48.9	MSSA	n/a	4.2%	61	1.0	15.9	0.083	0.18
1	16	male	Non-Hispanic White	17.7	52	yes	4.0	MOX, PIP, TOB	yes	70.6	MSSA	R: | S: OXA, CFZ, CIP, CLI, LIN, VAN, TET, TMP	none detected	61	2.2	10.8	0.039	0.11
1	16	male	Non-Hispanic White	19.1	63	no	n/a	MOX, PIP, TOB	n/a	52.9	MSSA	R: | S: OXA, CFZ, CIP, CLI, LIN, VAN, TET, TMP	none detected	40	0.9	10.4	0.099	0.58
2	14	male	Non-Hispanic White	n/a	68	no	n/a	DOX, LIN, TOB	no	40	MSSA	n/a	none detected	60	1.4	11.2	0.069	0.22
2	14	male	Non-Hispanic White	15.9	67	no	n/a	DOX, LIN, TOB	no	41.6	n/a	n/a	none detected	61	2.6	24.3	0.235	0.49
3	20	male	Non-Hispanic White	18.2	38	yes	30.0	CIP,‡ COL, TOB	yes	65.3	MSSA	R: CIP | S: OXA, CFZ, CLI, LIN, VAN, TET, TMP	none detected	40	0.9	14.9	0.230	0.97
4	14	male	Hispanic	19.1	50	no	n/a	TOB	no	68.1	MSSA	R: CLI | S: OXA, CFZ, LIN, VAN, TET, TMP	none detected	63	0.8	20.4	0.461	0.88
4	14	male	Hispanic	20.1	36	no	n/a	TOB	no	66.6	MSSA	R: CLI, TMP | S: OXA, CFZ, LIN, VAN, TET	none detected	60	1.1	20.2	0.395	0.8
5	16	female	Hispanic	16.5	22	yes	10.0	CFZ, TOB	no	NA	MSSA	R: | S: OXA, CFZ, CIP, CLI, LIN, VAN, TET, TMP	n/a	62	0.7	28.0	0.618	0.87
5	16	female	Hispanic	16.5	25	yes	35.0	CFZ, TOB	no	NA	MSSA	R: | S: OXA, CFZ, CIP, CLI, LIN, VAN, TET, TMP	n/a	60	1.1	19.1	0.244	0.51
5	16	female	Hispanic	17.29	20	no	n/a	AZT, CIP, TOB	yes	41.5	MSSA	n/a	none detected	60	1.5	19.0	0.211	0.45
6	9	female	Non-Hispanic White	14.1	69	yes	1.0	AZT, COL, PRI, TOB	no	NA	n/a	n/a	n/a	65	0.6	19.6	0.217	0.39
7	14	female	African-American	17.7	42	yes	12.0	AMI, AZT, CFP, TOB	yes	61.7	n/a	R: CIP | S: OXA, CFZ, CLI, LIN, VAN, TET, TMP	none detected	64	0.8	21.1	0.054	0.075
8	11	male	Hispanic	19.6	118	no	n/a		no	60.7	MSSA	R: | S: OXA, CFZ, CLI, LIN, VAN, TET, TMP	none detected	63	1.0	22.4	0.157	0.25
8	12	male	Hispanic	20.43	85	no	n/a		no	54	MRSA	R: | S: OXA, CLI, LIN, VAN, TMP	none detected	50	1.7	0.7	0.033	1.7

Table S1. Cont.

Patient	Age	Sex	Race	BMI, kg/m^2	FEV1%	Pulmonary exacerbation	Hospital day no.	Active antibiotics*	*P. aeruginosa* present	*Staphylococcaceae*, %	Type	*S. aureus* clinical culture antibiotic resistance (R)/ susceptability (S)†	*Xanthomonadaceae*	Incubation time, min	Sample weight, g	$^2F_{w_{eq}}$, atom%	$^2F_{fa}$, atom%	*S. aureus* growth rate, 1/d
8	12	male	Hispanic	21.32	94	no	n/a		no	NA	MSSA	R: | S: OXA, CLI, LIN, VAN, TMP	n/a	45	1.3	0.7	0.025	1.1
9	14	male	Hispanic	19.6	84	no	n/a		yes	54.8	MSSA	n/a	none detected	63	1.0	21.3	0.399	0.72
10	13	female	Hispanic	21.2	106	yes	4.0	ITR, OXA	no	47.9	MSSA	R: | S: OXA, CFZ, CIP, CLI, LIN, VAN, TET, TMP	none detected	62	0.6	21.2	0.100	0.16
11	17	male	Hispanic	17.3	67	yes	n/a	COL, TOB	no	70.8	MSSA	R: CLI | S: OXA, CFZ, CIP, LIN, VAN, TET, TMP	none detected	61	0.8	19.6	0.173	0.33
11	17	male	Hispanic	17.5	80	yes	8.0	COL, PIP, TOB	no	64.2	MSSA	R: CLI | S: OXA, CFZ, CIP, LIN, VAN, TET, TMP	none detected	60	0.8	19.9	0.101	0.18
11	17	male	Hispanic	17.3	64	yes	2.0	AMI, COL, PIP, TOB	no	62.6	MSSA	R: CLI | S: OXA, CFZ, CIP, LIN, VAN, TET, TMP	none detected	42	0.5	19.5	0.042	0.088
11	17	male	Hispanic	17.3	74	yes	6.0	AMI, COL, PIP, TOB	n/a	64.3	n/a	R: CLI | S: OXA, CFZ, CIP, LIN, VAN, TET, TMP	none detected	46	0.7	17.0	0.014	0.0088
12	12	male	Hispanic	n/a	72	yes	n/a	AZT, CLI*, TOB	yes	43.2	MRSA	R: OXA, CFZ, CLI | S: LIN, VAN, TET, TMP	none detected	63	0.8	19.9	0.541	1.1
12	12	male	Hispanic	n/a	70	yes	1.0	AZT, PIP, TOB, VAN	yes	69	MRSA	R: OXA, CFZ, CLI | S: LIN, VAN, TET, TMP	none detected	60	0.3	18.0	0.044	0.071
12	12	male	Hispanic	n/a	70	yes	1.0	AZT, PIP, TOB, VAN	yes	60.6	MRSA	R: OXA, CFZ, CLI | S: LIN, VAN, TET, TMP	none detected	61	0.5	20.2	0.067	0.11
12	12	male	Hispanic	16.8	71	no	n/a	AZT, TET, TOB	yes	49.8	MRSA	R: OXA, CFZ, CLI | S: LIN, VAN, TET, TMP	none detected	60	1.0	19.0	0.159	0.32
12	12	male	Hispanic	16.7	61	no	n/a	AZT, TOB	yes	46.8	MRSA	R: OXA, CFZ, CLI | S: LIN, VAN, TET, TMP	none detected	61	0.7	10.3	0.041	0.11
13	11	male	Non-Hispanic White	18.4	81	no	n/a		no	60.4	MRSA	R: OXA, CFZ, CIP, CLI | S: LIN, VAN, TET, TMP	none detected	61	0.5	19.2	0.556	1.2
13	11	male	Non-Hispanic White	17.7	78	no	n/a		no	50.4	MRSA	R: OXA, CFZ, CIP, CLI | S: LIN, VAN, TET, TMP	none detected	63	0.6	19.5	0.210	0.39
14	16	male	African-American	20.2	69	yes	2.0	MER, TOB, VAN	no	58.7	MRSA	R: OXA, CFZ | S: CIP, CLI, LIN, VAN, TET, TMP	none detected	47	1.0	22.8	0.013	0.0038

Table S1. Cont.

Patient	Age	Sex	Race	BMI, kg/m^2	FEV1%	Pulmonary exacerbation	Hospital day no.	Active antibiotics*	*P. aeruginosa* present	*Staphylococcaceae*, %	Type	*S. aureus* clinical culture antibiotic resistance (R)/ susceptability (S)†	*Xanthomonadaceae*	Incubation time, min	Sample weight, g	$^2F_{w_{eq}}$, atom%	$^2F_{fa}$, atom%	*S. aureus* growth rate, 1/d
14	16	male	African-American	19.9	71	yes	6.0	MER, TOB, VAN	no	NA	MRSA	R: OXA, CFZ | S: CIP, CLI, LIN, VAN, TET, TMP	n/a	60	0.6	22.1	0.092	0.15
14	16	male	African-American	20.2	75	yes	14.0	MER, TOB, VAN	no	43.2	MRSA	R: OXA, CFZ | S: CLI, LIN	none detected	60	0.9	22.2	0.135	0.23
14	17	male	African-American	19.7	80	no	n/a	TMP	no	63.8	MRSA	R: OXA, CFZ | S: CIP, CLI, LIN, VAN, TET, TMP	none detected	60	0.9	11.3	0.122	0.4
15	13	female	Hispanic	18.6	47	no	n/a	AZT, TOB	yes	55.6	n/a	n/a	none detected	41	0.9	9.9	0.057	0.32
16	12	female	Hispanic	21.1	96	no	n/a	AMO	no	55.5	MSSA	R: | S: OXA, CFZ, CIP, CLI, LIN, VAN, TET, TMP	none detected	60	0.7	5.4	0.158	1.1

n/a indicates instances where no data was available.

*Antibiotics the patient was getting at the time: AMI, amikacin; AMO, amoxicillin/clavulanic acid; AZT, inhaled aztreonam; CFP, cefepime; CFZ, cefazolin; CIP, ciprofloxacin; CLI, clindamycin; COL, colistin; DOX, doxycycline; ETH, ethambutol; ITR, itraconazole; LIN, linezolid; MER, meropenem; MOX, moxifloxacin; OXA, oxacillin; PIP, piperacillin/tazobactam; PRI, primaxin/imipenem/cilastatin; TET, tetracycline; TMP, trimethoprim/sulfamethoxazole; TOB, tobramycin; VAN, vancomycin.

†Only antibiotics actually used for patient treatment during this study are listed (see abbreviations above). Also typically tested but not used in treatment and therefore excluded from the table for clarity were ampicillin/sulbactam, erythromycin, levofloxacin, cephalexin, rifampin, and benzylpenicillin, all of which had very high incidence of *S. aureus* resistance.

‡These antibiotics were reported as ineffective (R category) in the susceptibility data for the respective sample and were therefore not considered as being effective against *S. aureus* (e.g., in Fig. 3).